CHAPTER VI
ROLES OF RUTHENIUM AND ITS PARTICLE SIZES IN CATALYTIC PYROLYSIS OF WASTE TIRE

6.1. Abstract

The catalytic pyrolysis of waste tire with Ru/SBA-1 catalysts was carried out. The roles of ruthenium were elucidated since the support, a pure silica SBA-1 synthesized via silatrane route, was proven to be catalytically inactive and its structure was retained after pyrolysis. Ruthenium clusters increased the yield of gaseous products, approximately 2 times as compared to thermal pyrolysis, at the expense of the liquid yield. In addition, the presence of ruthenium sites led to an obvious reduction in the concentration of poly- and polar-aromatics and also a shift of hydrocarbon distribution to the lighter fractions. A series of 1%Ru/SBA-1 catalysts having ruthenium particles sizes in the range of 2.5 nm to 4.5 nm was successfully prepared, as revealed from CO-chemisorption and TEM results. The catalytic activity of these Ru-based catalysts was found to be strongly dependent on the size of their ruthenium particles. The decrease in ruthenium particle size in the tested range increased the catalytic activity, in terms of poly- and polar-aromatic reduction and light oil production. The observed phenomena were explained in relation with catalyst characterization results.

6.2. Introduction

The main advantage of tire pyrolysis is that all of its products, i.e. a carbonaceous char, oil and a gas fraction, have potential to be utilized [1]. Among them, pyrolytic oil has attracted much more attentions due to its high heating value [2] and its property, which was reported to be similar, to a certain extent, to that of commercial naphtha [3]. However, the major obstacle that has limited the application of this oil as fuel is its high concentration of aromatics, especially polycyclic aromatic compounds [3]. Moreover, pyrolytic oil has been shown to contain a considerable amount of sulfur-containing compounds [4]. And the low resistance to

sulfur poisoning is one of the major drawbacks of noble metal-supported catalysts. Interestingly, sulfur tolerance may be enhanced by modifying the physicochemical characteristics of the metal atoms by (i) using acidic carriers, (ii) alloying with other metals, or (iii) changing the metal particle size [5]. Different metal particle sizes can be obtained by controlling the catalyst preparation conditions/methods [6].

Recently, we have reported the high activity of Ru-supported mesoporous MCM-41 for poly- and polar-aromatics reduction, and simultaneously for the production of light oil from waste tire pyrolysis [7]. The high activity of Ru/MCM-41 catalyst was proposed to be the combination effects of its bifunctionality contributed from metal and acid sites. However, the complex structure of tire, together with the presence of bifunctionality of the catalysts, makes it difficult to distinguish the role(s) of metal and acid sites during catalytic pyrolysis. Meanwhile, understanding the role of each individual site might help designing a better catalyst.

This study was carried out to investigate the roles of ruthenium during waste tire pyrolysis. The influences of ruthenium particle size on the catalytic activity of Ru-based catalysts were also studied.

6.3. Experimental

6.3.1 Catalyst Preparation

To synthesize SBA-1, silatrane was first synthesized using the method of Wongkasemjit's group [8]. The silatrane precursor was added to a solution containing NaOH, and H_2SO_4, followed by adding a solution of water and CTAB with vigorous stirring [9]. Water was added to this mixture prior to aging at room temperature for 2 days to form a white precipitate. The product was filtered and washed with water. Then, the white solid was dried at room temperature and calcined at 580°C for 6 hours (0.5°C/min) to obtain mesoporous SBA-1.

Ru-supported catalysts were prepared using conventional wetness impregnation technique. An appropriate amount of precursor solution of $RuCl_3.xH_2O$, purchased from FLUKA, was dropped to the SBA-1 to obtain 1 %wt of Ru, followed by drying in an oven at 110°C for 3 hours. In order to obtain Ru/SBA-1 catalysts with different ruthenium particle sizes, the obtained dried sample was divided into 3

portions, which were calcined under different heating rates (1°C/min, 5°C/min, and 10°C/min) from room temperature to 580°C. Subsequently, all samples were pelletized and sieved to obtain particle sizes in the range of 400- 425 μm. Prior to catalytic activity testing, all catalysts were reduced by hydrogen at 400°C for 3 hours.

6.3.1 Catalyst Characterization

XRD patterns were obtained using the Riguku D/Max 2200H with a scanning speed of 0.5 degree/min and 2θ from 1.5 degree to 60 degree. The composition of the Ru on the support was determined by the Inductively Coupled Plasma (ICP) technique (Perkin Elmer Optima 4300 PV). The surface area, pore volume and pore size distribution of the studied catalysts were characterized by N_2 physical adsorption using a Sorptomatic 2900 equipment. Carbon monoxide chemisorption was carried out in a Micromeritics 2900 apparatus at room temperature, after the *in-situ* reduction of sample at 500°C (10°C/min) for 1 hour, under a flow of H_2. Dispersion data was calculated by assuming a stoichiometry of CO/Ru =1 [10]. SEM and TEM images were recorded by a JEOL 2010 and JEM 2100 instrument, respectively. For determination of particle size by TEM, the mean size of Ru particles was calculated on the basis of size measurements of 300-500 for each sample. Temperature programmed techniques including H_2-TPR, TPD-H_2, and TPO were conducted using the same Micromeritics 2900. For TPD-H_2, about 0.1g of sample was first pretreated in He at 550°C for 30 minutes. Then, the system was cooled to 30°C, and the H_2 adsorption was performed for 1 hour, followed by He purging for 30 minutes. The TPD-H_2 was started from 30°C to 500°C with a heating rate of 5°C/min. TPR-H_2 of Ru-supported catalysts was conducted from room temperature to 500°C with a heating rate of 5°C/min after pre-treatment of sample at 150°C under He flow for 1 hour. TPO was performed from room temperature to 900°C (10°C/min), and the final temperature was held for 30 minutes. The amount of coke was then determined from the area under the curve and calculated by the software equipped with the machine. The sulfur contents in waste tire and in the spent catalysts were determined by elemental analysis (LECO, US).

6.3.3 Pyrolysis of Waste Tire

The detail of pyrolysis process was described elsewhere [11]. Briefly, a tire sample was pyrolyzed in the lower zone of the reactor (500°C), and then the

evolved product was carried to the upper zone (350°C) packed with a catalyst. The obtained product was next passed through a condensing system to separate incondensable compounds from the liquid product. The solid and liquid products were weighed to determine the product distribution. The amount of gas was then determined by mass balance. The gaseous product was analyzed by a GC equipped with an FID. The liquid product was first dissolved in n-pentane to precipitate asphaltenes. The obtained maltenes was analyzed by FTIR and liquid adsorption chromatography [12], in which saturated hydrocarbons, mono-, di-, poly-, and polar-aromatics were fractionated. Finally, a SIMDIST GC was used to analyze the obtained maltenes and hydrocarbon fractions according to the ASTM D2887 method to determine the simulated true boiling point (TBP) curves. The curves were then cut into petroleum fractions, based on their boiling point ranges, including naphtha (<200°C), kerosene (200°C-250°C), light gas oil (250°C – 300°C), heavy gas oil (300°C-370°C), and residue (>370°C).

6.4. Results and Discussion

6.4.1 SBA-1 as the Selected Support

In order to clearly determine the roles of ruthenium and the effects of ruthenium particle size of Ru-supported catalyst in the catalytic pyrolysis of waste tires, a selected support should not play any role on chemical reactions. Additionally, to obtain a high metal dispersion for a metal-supported catalyst, the use of a zeolite, especially the one having large surface area, is commonly suggested. Moreover, a pure silica material has been shown to be inactive for the conversion of used tire rubber into hydrocarbon products [13]. Consequently, in this study, a silica SBA-1 was first synthesized *via* the silatrane route [9]. The accomplishment of the material synthesis was confirmed by XRD and N_2-physical adsorption results. The surface area and pore volume of the synthesized SBA-1 are 1,428 m^2/g and 0.72cm^3/g, respectively, which are similar to the values from the reference [9].

The experiment results of thermal and catalytic pyrolysis using SBA-1 as a catalyst are depicted in Figure 6.1. It can be seen that the yield of solid product is similar in both runs (Figure 6.1A). This is because of the fact that the pyrolysis

conditions were kept constant and the tire was reported to be completely decomposed at 500°C [14]. As compared to non-catalytic case, the use of SBA-1 insignificantly influences the product yields because the yields of gas and liquid products in the two runs are comparable. In addition, the concentrations of saturated hydrocarbons, mono-, di-, poly- and polar-aromatics, analyzed by liquid adsorption chromatography, of the two derived oils are quite similar (Figure 6.1B). Furthermore, the TBP curves of the two oils are mostly overlapped (Figure 6.1C). Thus, it is safe to conclude that SBA-1 is catalytically inactive for waste tire pyrolysis.

6.4.2 Roles of Ruthenium during Catalytic Pyrolysis of Waste Tire

1%Ru-supported SBA-1 catalyst was prepared, and its catalytic activity was tested for understanding the role of ruthenium in the waste tire pyrolysis. The amount of ruthenium loaded on the SBA-1 support is confirmed by ICP analysis. No loss in the crystallinity of the SBA-1 is detected in the XRD pattern of the prepared 1%Ru/SBA-1 sample. Note that the SBA-1 was proven to be catalytically inactive for waste tire pyrolysis; thus, from this point, the influences of 1%Ru/SBA-1 will be presented by comparing directly to the thermal-pyrolysis.

The results of experiments with and without 1%Ru/SBA-1 are given in Figure 6.2. The results include the product yields, petroleum cuts, and compositions of the derived oils. Figure 6.2A shows that 1%Ru/SBA-1 decreases the yield of oil in accordance with an increase in the yield of gaseous products. Namely, the gas yield increases from ~10 %wt to ~20 %wt. Figure 6.2B shows the petroleum fractions in the pyrolysis oils. A high concentration of heavy fractions, i.e. residues and heavy gas oil, is observed in the non-catalytic oil. The presence of 1%Ru/SBA-1 catalyst shifts the TBP curves to lower temperature, resulting in the increase in light fractions. The content of light fraction (boiling point < 250°C) increases from approximate 50 wt% to over 70 wt%. Figure 6.2C indicates that 1%Ru/SBA-1 strongly influences the compositions of the pyrolysis oils. As compared to non-catalytic oil, the contents of poly- and polar-aromatic hydrocarbons (PPAHs) are much lower. The reduction of these heavy HCs caused by the presence of Ru-based catalysts is further confirmed by observing the results obtained from FTIR analysis (Figure 6.2D). This figure presents the FTIR spectra of the oils in the wave number corresponding to the polycyclic aromatic range [15,16]. The intensity of peaks at

700cm^{-1} and 740cm^{-1} in the spectrum of the oil produced over 1%Ru/SBA-1 is obviously lower than that of the non-catalytic case, indicating a lower concentration of polycyclic HCs [16].

The formation of PPAHs from the pyrolysis of waste tire was reported to occur through the Diels-Alders reaction and aromatization [4,17,18]. And a poly-aromatic compound, such as phenathrene, was formed after the formation of naphthalene, a di-aromatic compound. Moreover, no evidence proving the direct formation of aromatics from cyclization of alkanes was observed [17]. The presence of ruthenium clusters in this study drastically decreases PPAHs (Figure 6.2C). Due to the fact that the nature of ruthenium is highly active for catalyzing hydrogenation reaction [5]; thus, it might decrease PPAHs either by: (i) converting their intermediates to smaller molecules preventing their formation (*first route*), or: (ii) transforming them to other types of molecules, most likely through hydrogenating (*second route*).

If the first route is really the case, then the content of di-aromatics, intermediates of PPAHs, should be lower with respect to the thermal pyrolysis. However, for 1%Ru/SBA-1 catalyst, the reduction of PPAHs is accompanied with the increase in di-aromatics; thus, the occurrence of the first route is unlikely. Moreover, it has been reported that the hydrogenation of poly-aromatics is more preferable than their di-aromatic intermediates [19], and generally yields partial hydrogenated products [20]. This, together with the higher concentration of di-aromatics (for 1%Ru/SBA-1) with respect to thermal pyrolysis (Figure 6.2C), suggests that the reduction of PPAHs is more likely to occur by the second route. However, it should be noted that no evidence disproving the first route has been found. Therefore, it can be concluded that ruthenium decreases PPAHs by both ways, but the second route is more likely.

The presence of ruthenium clusters also decreases saturates in the derived oil (Figure 6.2C). This is well consistent with the results obtained from FTIR analysis (Figure 6.2E). The peak at 3030 cm^{-1} corresponds to the C-H stretch aromatic C, whereas the peak at 2920 cm^{-1} belongs to the CH stretch aliphatic [15]. And, the ratio between the intensity (I) of peak at 3030 cm^{-1} and 2920 cm^{-1} ($I_{3030cm-1}/I_{2920cm-1}$) relates to the concentration of saturates in oil [21]. It can be seen that as

compared to thermal pyrolysis, this ratio increases when 1%Ru/SBA-1 was used, indicating a lower concentration of saturates in the derived oil [22]. Usually, Ru-based catalyst is a good catalyst for hydrogenolysis reaction of hydrocarbons [5]. And, a consequence of hydrogenolysis generally is the production of light alkanes [23]. From the gas analysis from both thermal and catalytic pyrolysis in Figure 6.2F, the yields of methane, ethane, propane and mix-C_4 increase dramatically when 1%Ru/SBA-1 was used. Therefore, those saturates might be converted to the light gases, supporting that the deep hydrogenolysis reactions might have occurred [24], reducing saturates in the oil.

Up to this point, it has been proven that ruthenium cluster strongly influences the pyrolysis products, SBA-1 is catalytically inactive, and there is no loss of the crystallinity of this support after incorporation with ruthenium. However, the topology and/or morphology of a zeolite can be changed during reaction [25], which can also be the cause of catalytic activity change [25,26]. Therefore, it is essential to analyze the spent 1%Ru/SBA-1 catalyst to see if any change in the structure of the support has occurred, which would have contributed to the change on the activity. The coke deposited on the spent 1%Ru/SBA-1 was first removed by oxidation. Then, it was subject to analysis by means of XRD and SEM. It can be seen that its XRD pattern is similar to the fresh catalyst (Figure 6.3). Actually, no difference can be observed. In addition, the SEM image of the spent catalysts depicted in Figure 6.4A reveals the preservation of the SBA-1 structure. Therefore, it is safe to conclude that the structure of SBA-1 did not change during pyrolysis. As a consequence, the catalytic activity of 1%Ru/SBA-1 is only attributed to the ruthenium contribution.

Conclusively, ruthenium strongly increases the yield of gas in accordance with a reduction of the oil yield. Moreover, the presence of ruthenium also produces much lighter oil by decreasing poly- and polar-aromatics. Saturates in oil is also lessened possibly due to the high hydrogenolysis activity of ruthenium clusters.

6.4.3 Influences of Ruthenium Particle Sizes

6.4.3.1 Catalyst Characterization

XRD patterns of Ru/SBA-1 samples (not shown here) reveal the retaining of the support structure after incorporation with metal. And, neither

peak of ruthenium nor ruthenium compound is found in all XRD patterns. Probably, the concentrations of Ru on the surface of SBA-1 support are below the detectable range of the instrument and/or Ru is highly dispersed in all samples.

The metal particle size or the consequent dispersion is strongly dependent on the preparation condition, as expected (Table 6.1). The sample prepared under the highest heating rate during calcination has the biggest particle size, as determined by CO-chemisorption and TEM. A typical TEM image of the studied catalysts is illustrated in Figure 6.4B. For determination of particle size by TEM, the mean size of Ru particles was calculated on the basis of size measurements of 300-500 for each sample. The average particle size obtained from TEM is slightly lower than that obtained from CO-chemisorption for the same sample. However, the trend of the mean ruthenium particle size variation is identical.

Table 6.1 Physical-chemical properties of Ru-supported catalysts

	Ru (%wt)	Pore volume (cm^3/g)	Surface area (m^2/g)	Pore diameter (nm)	Dispersion (%)	Mean Ru particle size (nm)*	
						TEM	CO-chemisorption
SBA-1	-	0.72	1428	2.17	-	-	-
4.5Ru/SBA-1	1.02	0.67	1387	2.19	26.6	4.49	4.85
4.0Ru/SBA-1	0.98	0.68	1396	2.22	29.8	3.99	4.33
2.5Ru/SBA-1	0.99	0.71	1405	2.13	48.8	2.56	2.64

*Volume-area mean diameter

Table 6.1 also summarizes the physical-chemical properties of the studied Ru-based catalysts. The number in front of the sample name stands for its mean diameter of ruthenium particles obtained from TEM. From ICP analysis, the percentage of Ru in all samples is well consistent with the targeted value. Meanwhile, the surface area and pore volume of all samples decrease with the addition of ruthenium. However, the mean pore diameter of 4.0Ru/SBA-1 and 4.5Ru/SBA-1 samples is higher than that of SBA-1, possibly caused by the blockage of small pores by ruthenium particles leading to the increment of mean diameter. The pore blockage might also be the reason for the reduction in total pore volume.

H_2-TPR profiles of Ru-supported catalysts are displayed in Figure 6.5. From the figure, all profiles present two overlapped reduction peaks. The first peak at low temperature (around 195°C) is assigned to the Ru^{3+}/Ru^0 single step reduction, whereas the second peak located at high temperature (~ 230°C) comes from the reduction of RuO_2 [5]. The H_2-consumption curve of 2.5Ru/SBA-1 sample is broad, possibly due to the reduction of highly-dispersed ruthenium species located in different environments; and its high temperature peak is the clearest, indicating a high amount of ruthenium oxide. The signals of the 4.0Ru/SBA-1 and 4.5Ru/SBA-1 are clearly narrower than 2.5Ru/SBA-1, probably due to the poor dispersion of ruthenium in the two samples, leading to the formation of bigger particles [27], which is well consistent with CO-chemisorption and TEM results (Table 6.1). Moreover, all samples have similar ruthenium content; thus, the location of the peaks indicates the degree of metal support interaction. The stronger the metal support interaction, the more difficult it is to reduce the metal. And, a strong interaction between metal and support helps prevent sintering during reaction, resulting in a slower deactivation of the catalyst [5]. Among all samples, 2.5Ru/SBA-1 has the strongest interaction between metal and support indicated by its highest temperature of the reduction peak. This can be attributed to the its highest amount of RuO_2 that has strong ruthenium-oxygen-silica interactions [28,29].

In order to investigate the H_2 uptake of the reduced catalysts, the Ru-supported samples were subjected to TPD-H_2 analysis. The results are displayed in Figure 6.6. All samples show one hydrogen chemisorption peak locating at a temperature below 200°C. However, the location of the peak is different from sample to sample. The peak of TPD-H_2 profile of 2.5Ru/SBA-1 is located at the highest temperature. Considering the intensity of the peak which is the indication of hydrogen adsorption on the metal sites, the observed trend is 2.5Ru/SBA-1>> 4.0Ru/SBA-1> 4.5Ru/SBA-1. This is well consistent with the results obtained from CO-chemisorption and TEM. Namely, the sample, which shows the higher hydrogen uptake, has smaller ruthenium particles. When the particle is smaller, there exists the greater amount of accessible ruthenium atoms for hydrogen to adsorb; thus, increasing total hydrogen uptake.

6.4.3.2 Influences of Ruthenium Particle Size

As demonstrated in the previous section, a series of 1%Ru/SBA-1 catalysts having different ruthenium particle sizes was successfully prepared. As such, this section presents the influences of ruthenium particle size on the yield and nature of the obtained products, which are summarized in Figure 6.7.

Figure 6.7A illustrates the product distribution obtained from using Ru/SBA-1 catalysts having various ruthenium particle sizes. The size of ruthenium particle strongly affects the yield of gaseous product. The gas yield increases gradually at the expense of the yield of oil with decreasing ruthenium particle size. For instance, the yield of gaseous product increases from around 15 %wt to almost 25 %wt whereas the oil yield drops from around 40 %wt to 30 %wt when the ruthenium particle size decreases from 4.5 nm to 2.5 nm. The influence of ruthenium particle can be further depicted by the petroleum cuts as shown in Figure 6.7B. The decrease in ruthenium particle size causes a shift of hydrocarbons from heavy fractions *i.e.* residues and heavy gas oil (HGO) to lighter fractions, naphtha and kerosene. And the highest selectivity toward light fractions is observed over the smallest ruthenium particle containing sample, 2.5Ru/SBA-1. Figure 6.7C depicts the compositions of the derived oils, which reveals that the sample having the smallest ruthenium particle exhibits the highest activity for the reduction of PPAH compounds in the derived oil. And, increasing ruthenium particle size decreases the activity on PPAH reduction. The mechanism of hydrogenation reaction of aromatics was reported to involve the dissociative adsorption of H_2 on the metal sites [30]. Meanwhile, as revealed from catalyst characterization, the sample having smaller ruthenium particle size possesses higher hydrogen uptake (Figure 6.6). Therefore, 2.5Ru/SBA-1 exhibit higher hydrogenation activity as compared to the other Ru-supported catalysts due to its smallest ruthenium particle size (Table 6.1). As a consequence, the lowest concentration of PPAHs was detected in the oil obtained from using this catalyst.

As elucidated in Section 3.2, the ruthenium sites are the active sites for the reduction of PPAHs and saturates in the derived oils, possibly by hydrogenation and hydrogenolysis reactions, respectively. Moreover, the sample with the smallest particle size produces the oil having the highest selectivity toward

light fractions, *i.e.* naphtha and kerosene (Figure 6.7B), in accordance with the lowest concentration of PPAHs (Figure 6.7C). Besides, the yields of light alkane hydrocarbons in gaseous products increase gradually with decreasing ruthenium particle size (Figure 6.7D). These observations suggest the existence of greater hydrogenation and hydrogenolysis reactions [24] as the metal particle size decreases due to the increase of ruthenium specific surface area. Therefore, it is likely that the decreasing ruthenium particle enhances hydrogenation reactions, then, the hydrogenated species might be further converted into lower molecular weight compounds by thermal cracking and/or hydrogenolysis reactions. That explains the increment in light oil production with decreasing ruthenium particle size. In addition, the greater hydrogenolysis reactions also explain the decrease in saturated HC content in the obtained oils (Figure 6.7C). FTIR experiment (not shown here) further confirms the reduction in saturates in oil with decreasing ruthenium particle size.

The results of TPO experiments of spent SBA-1 and Ru-based catalysts are presented in Figure 6.8. SBA-1 sample shows a main oxidation peak at 300°C – 400°C, whereas the TPO curves of all Ru/SBA-1 samples consist of two peaks located at around 300°C and 500°C. The first peak located at low temperature (~300°C) is most likely due to the oxidation of adsorbed hydrocarbon species, which could be formed from condensed polycyclic compounds [31]. And the second peaks at 500°C – 600°C, corresponding to the oxidation of deposited carbon species [31], are obviously distinguishable. In addition, a shift of the second peaks to higher temperature with decreasing ruthenium particle size is observed.

Table 6.2. Coke and sulfur in the spent catalysts

Spent Catalysts	SBA-1	2.5Ru/SBA-1	4.0Ru/SBA-1	4.5Ru/SBA-1
Coke (g/g cat)	0.027	0.061	0.098	0.112
Sulfur (%wt)	-	1.75	2.12	2.20

The quantitative TPO analysis data calculated the temperatures in the range of 250°C – 850°C are shown in Table 6.2. As such, clearly the Ru-based

catalysts produce the higher amount of coke than SBA-1 does. In addition, among Ru-supported samples, there exists a trend of increasing coke formation with the increasing of ruthenium particle sizes. Namely, the amount of coke increases in the following order: SBA-1 < 2.5Ru/SBA-1 < 4.0Ru/SBA-1 < 4.5Ru/SBA-1.

Elemental analysis gives the sulfur content in the feed (waste tire) is 1.56 %wt. Consequently, during pyrolysis of waste tire, a considerable amount of sulfur-containing polar-aromatic compounds is produced. And these sulfur-containing compounds can deactivate the noble metal-supported catalysts by the strong bonding between the sulfur atoms and metal atoms [5,32]. The metal-support interaction plays an important role in changing the strength of the bonding interaction between sulfur and metal [20,32-34]. In addition, a stronger interaction between metal and support also helps prevent sintering during reaction, resulting in a slower deactivation of the catalyst [5]. Besides, the sulfur tolerance might also be enhanced by changing the metal particle size [5]. According to the results of elemental analysis for sulfur contents in the spent catalysts given in Table 6.2, 2.5Ru/SBA-1 exhibits the highest sulfur tolerance among Ru-supported catalysts due to its lowest sulfur content, which is probably caused by its strongest interaction between metal and support and smallest ruthenium particle. Consequently, 2.5Ru/SBA-1 exhibits the highest catalytic activity with the least coke formation. The other samples, which have bigger ruthenium particles, display much lower catalytic activity due to their low dispersion and resistance to coke formation.

6.5 Conclusions

The roles of ruthenium and the effects of its particle sizes in the catalytic pyrolysis of waste tire with Ru/SBA-1 catalysts have been studied. SBA-1 was selected to be used as the support since it was proven to be relatively catalytically inactive and its structure remained unchanged after reaction. Ruthenium clusters were the active sites for poly- and polar-aromatic hydrocarbons (PPAHs) reduction. And, ruthenium sites also decreased saturates in the derived oils. The conversion of these PPAHs and saturated compounds to the lighter one with the presence of ruthenium sites resulted in the greater light oil production as well as the increment of

the yield of gaseous products.

Ruthenium particle sizes strongly influenced the catalytic activity of Ru-supported catalysts. Poly- and polar-aromatic reduction activity increased with decreasing ruthenium particles. Consequently, the content of light fractions in the derived oil also increased with decreasing ruthenium particles. The increase in catalytic activity with decreasing particle size was explained by the higher dispersion, resulting in the increase in H_2 uptake, and by the stronger interaction between metal and support, leading to the better coke resistance.

6.6 Acknowledgements

The authors would like to gratefully thank Dr. Walairat Tanglumlert for her great helps in SBA-1 synthesis. Center of excellence for petroleum, petrochemical, and advanced materials, Chulalongkorn University, Thailand, the Thailand Research Fund (TRF), the Chulalongkorn University's Research Unit of "Syntheses and Applications of Organometallics" and The Graduate Scholarship Program for Faculty Members from Neighboring Countries, Chulalongkorn University are acknowledged for the partial financial support.

6.7 References

[1]. P.T. Williams and A.J. Brindle, J. Anal. Appl. Pyrolysis 67 (2003) 143-164

[2]. A.M. Cunliffe, P.T. Williams, J. Anal. Appl. Pyrolysis 44 (1998) 131-152

[3]. B. Benallal, C. Roy, H. Pakdel, S. Chabot, M.A. Poirier, Fuel 74 (1995) 1589-1594

[4]. Nguyễn Anh Dũng, Sujitra Wongkasemjit, Sirirat Jitkarnka, Influences of pyrolysis temperature and Pt-loaded catalysts on the polar-aromatic content in tire-derived oils, Appl. Catal. B: Environ. In Press DOI:10.1016/j.apcatb.2009.05.038

[5]. D. Eliche-Quesada, J.M. Merida-Rboles, E. Rodriguez-Caslellon, A. Jimenz-Lopez, Appl. Catal. B: Environ. 65 (2006) 118-126.

[6]. H.–H. Chen, S.-C. Shen, X. Chen, S. Kawi, Appl. Catal. B: Environ. 50

(2004) 37-47.

[7]. Nguyễn Anh Dũng, Sujitra Wongkasemjit, Sirirat Jitkarnka, On the catalytic pyrolysis of waste tire using Ru-supported silica MCM-41, Manuscript submitted to J. Anal. Appl. Pyro.

[8]. W. Charoenpinijkarn, M. Sawankruhasn, B. Kesapabutr, S. Wongkasemjit, A.M. Jamieson, Eur. J. Polym. 37 (2001) 1441–1448

[9]. W. Tanglumlert, T. Imae, T.J. White, S. Wongkasemjit, Matter. Lett. 62 (2008) 4545-4548

[10]. T. Mitsui, K. Tsutsui, T. Matsui, R. Kikuchi, K. Eguchi, Appl. Catal. B: Environ. 81 (2008) 56-63.

[11]. N.A. Dũng, A. Mhodmonthin, S. Wongkasemjit, and S. Jitkarnka, J. Anal. Appl. Pyro. 85 (2009) 338-344

[12]. G. Sebor, J. Blaz ek, M.F. Nemer, J. Chromatogr A, 847 (1999), 323-330.

[13]. G. S. Miguel, J. Aguado, D.P. Serrano, J.M. Escola, Appl. Catal. B: Environ. 64 (2006) 209-219.

[14]. C. Berrueco, E. Esperanza, F.J. Mastal, J. Ceamanos, P. Garcia-Baicaicoa, J. Anal. Appl. Pyrolysis 74 (2005) 245-253.

[15]. C.A. Islas-Flores, E.Buenrostro-Gonzalez, C.Lira-Galeana, Fuel 85 (2006) 1845-1850.

[16]. C. Jager, F. Huisken, H. Mutschke, Th. Henning, W. Poppitz, I. Voicu, Carbon 45 (2007) 2981-2994.

[17]. P.T. Williams and D.T. Taylor, Fuel 72 (1993) 1469-147.

[18]. P.T. Williams and R.P. Bottrill, Fuel 74 (1995) 736-742

[19]. S. Jongpatiwut, Z. Li, D. E. Resasco, W.E. Alvarez, Ad L. Sughrue, G.W. Dodwell, Appl. Catal. A: Gen. 262 (2004) 241-253.

[20]. M. Jacquin, D.J. Jones, J. Roziere, S. Albertazzi, A. Vaccari, M. Lenarda, L. Storaro, R. Ganzerla, Appl. Catal. A: Gen. 251 (2003) 131-141.

[21]. S.H. Wang and P.R. Griffiths, Fuel 64 (1985) 229-265.

[22]. C.A. Islas-Flores, E.Buenrostro-Gonzalez, C.Lira-Galeana, Fuel 85 (2006) 1845-1850.

[23]. G. Kinger, H. Vinek, Appl. Catal. A: Gen. 218 (2001) 139-149.

[24]. V.M. Akhmedov, S. Al-Khowaiter, Appl. Catal. A: Gen. 197 (2000) 201-

212.

[25]. T. Wongkerd, A. Luengnaruemitchai, S. Jitkarnka, Appl. Catal B: Environ 78 (2008) 101-111.

[26]. Y. J. Lee, J.-H. Kim, S.H.Kim, S.B.Hong, G. Seo, Appl. Catal. B: Environ. 83 (2008) 160-167.

[27]. D. Eliche-Quesada, M.I. Marcias-Ortiz, J. Jimenez-Jimenez, E. Rodriguez-Castellon, A. Jimenez-Lopez, J. Mole. Catal. A: Chemical 255 (2006) 41-48.

[28]. A. Mazzieri, F. Coloma-Pascual, A. Arcoya, P.C. L'Argentiere, N.S. Figoli, Appl. Surf. Sci. 210 (2003) 222-230.

[29]. V.G. Komvokis, G.E. Marnellos, I.A. Vasalos, K.S. Triantafyllidis, Appl. Catal. B: Environ. 89 (2009) 627-634.

[30]. H. Du, C. Fairbridge, H. Yang, Z. Ring, Appl. Catal. A: Gen. 294 (2005) 1-21.

[31]. J. Zheng, J. Guo, C. Song, Fuel. Proces. Techno. 89 (2008) 467-474.

[32]. C. Naccache, M. Primet, M.V. Mathieu, J. Catal. 121 (1973) 266

[33]. W.M.H. Sachtler, A.Y.u.Stakneev. Catal. Today 12 (1992) 283-295.

[34]. D.Poondi and A.A. Vannice, J. Catal. 161 (1996) 742-751.

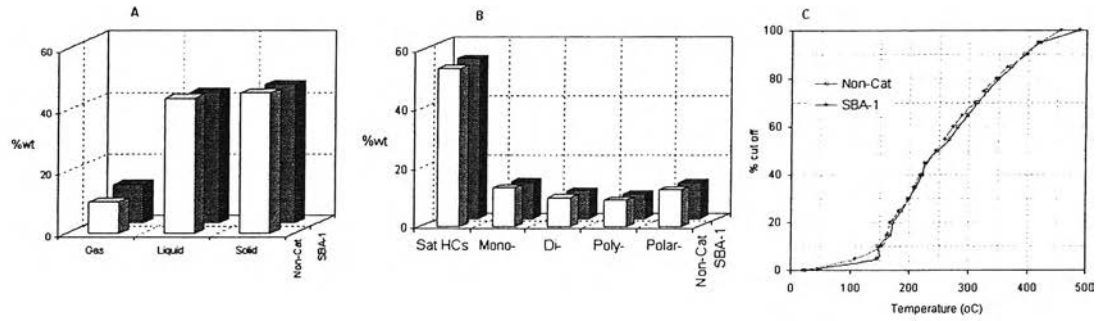

Figure 6.1 Effects of SBA-1 on the pyrolysis products: (A) Product distribution, (B) Liquid compositions, and (C) True Boiling Point Curves.

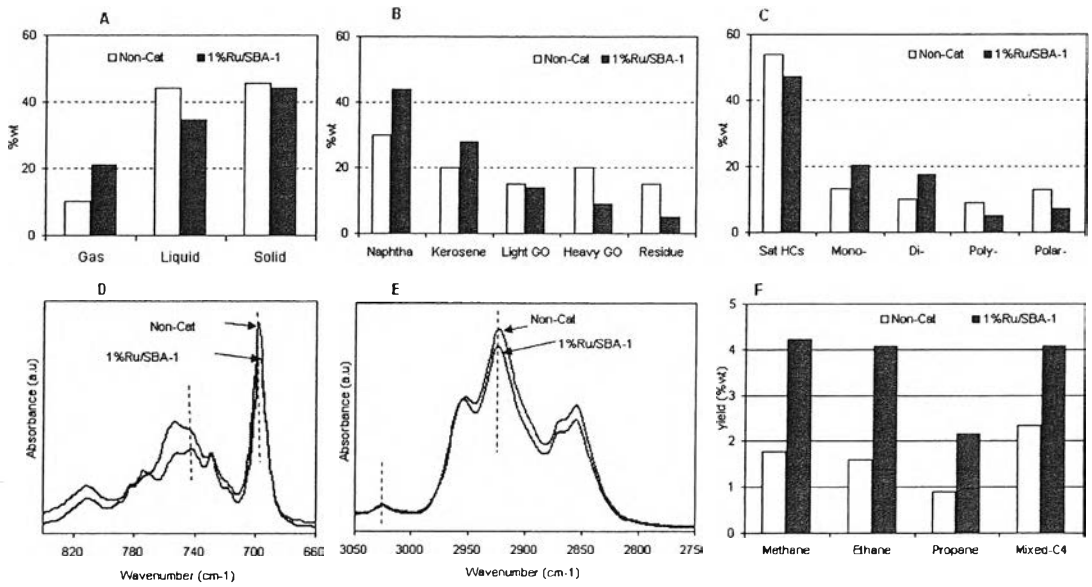

Figure 6.2 Effects of 1%Ru/SBA-1 on the pyrolysis products: (A) Product distribution, (B) Petroleum cuts, (C) Liquid composition, (D) FTIR in the aromatic range, (E) FTIR in the saturates range, and (F) Light alkanes yield.

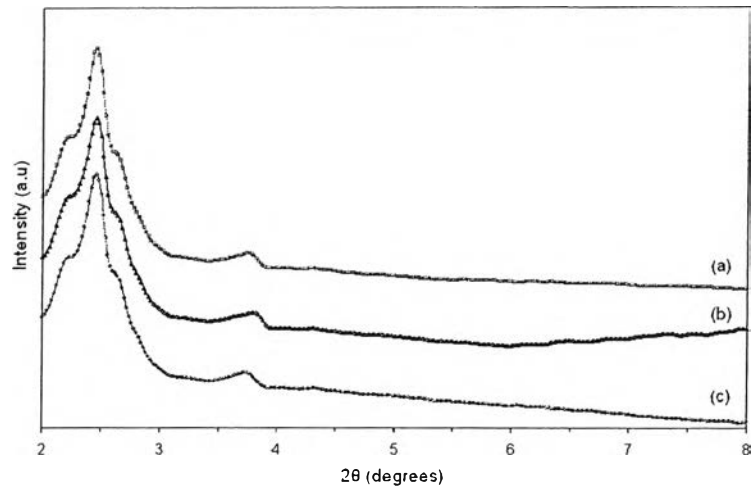

Figure 6.3 XRD patterns (a) SBA-1, (b) Fresh 1%Ru/SBA-1, and (c) Spent 1%Ru/SBA-1 after coke removal.

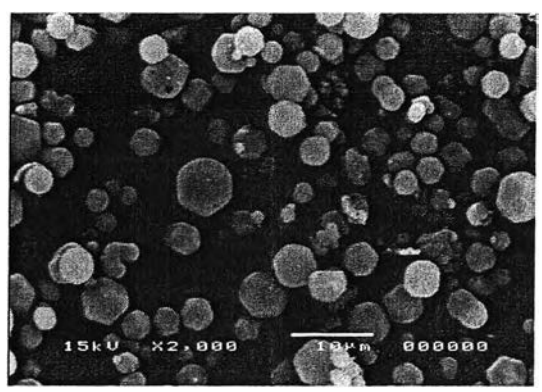

(A) Spent 1%Ru/SBA-1

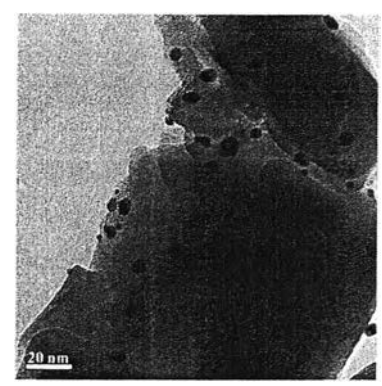

(B) TEM image of 4.5Ru/SBA-1

Figure 6.4 (A) SEM image the spent 1%Ru/SBA-1 after coke removal; (B) TEM image of 4.5Ru/SBA-1

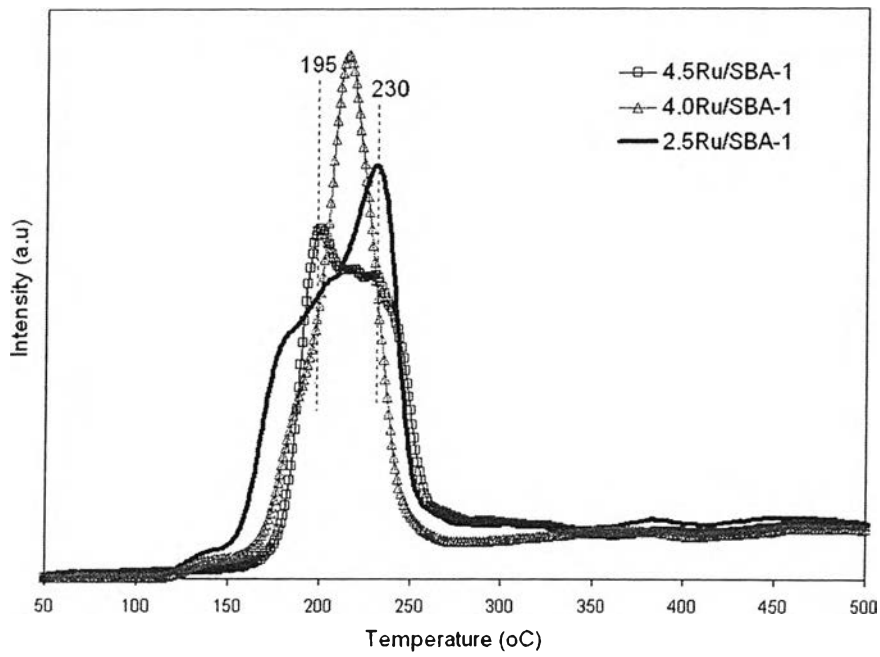

Figure 6.5 H_2-TPR profiles of Ru/SBA-1 catalysts.

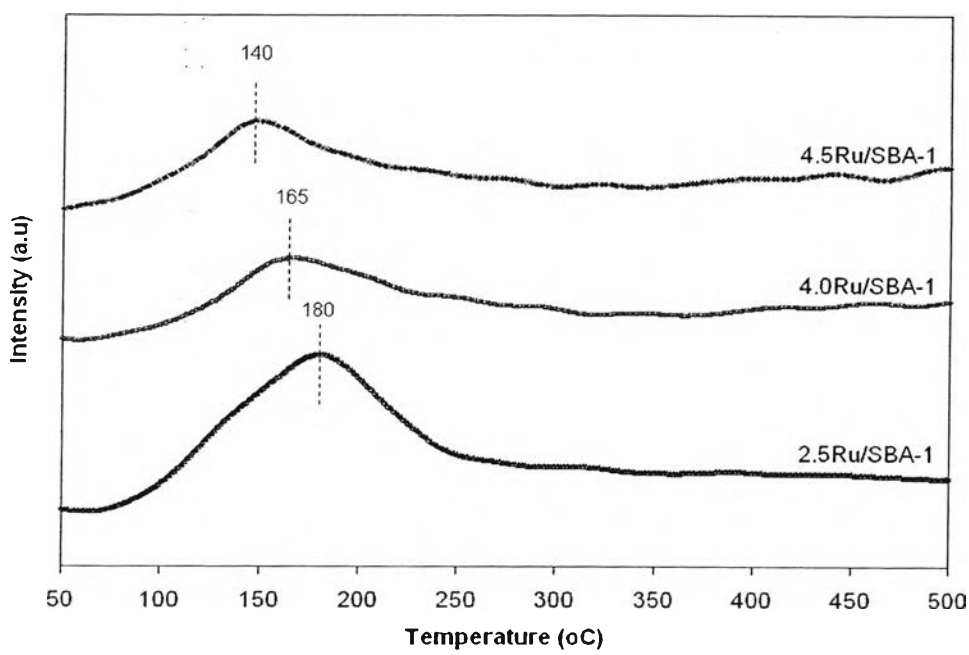

Figure 6.6 Hydrogen TPD profiles of reduced Ru/SBA-1 catalysts.

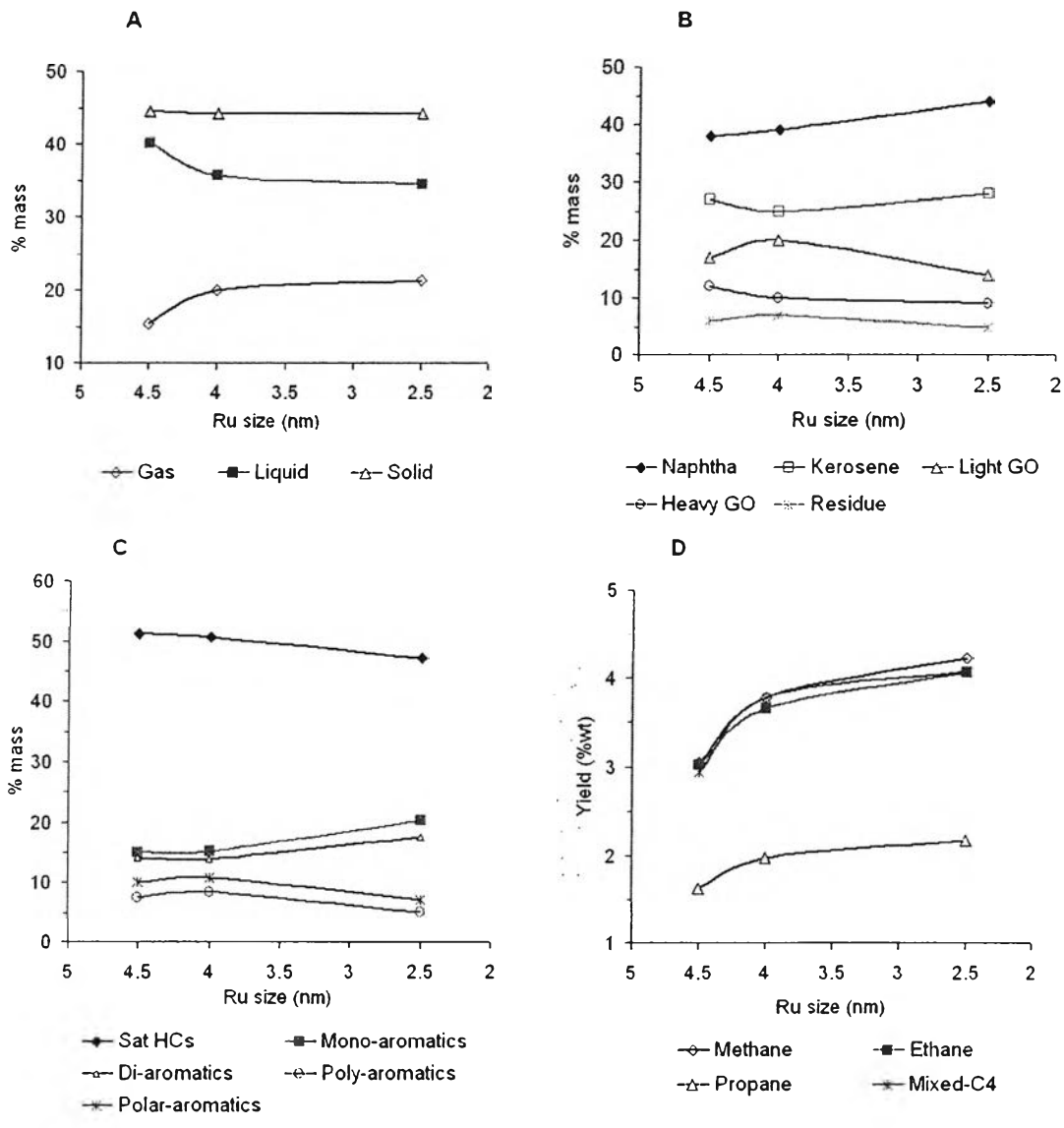

Figure 6.7 Influences of ruthenium particle size on pyrolysis products: (A) Product distribution, (B) Petroleum cuts, (C) Liquid compositions, and (D) Light alkanes yield.

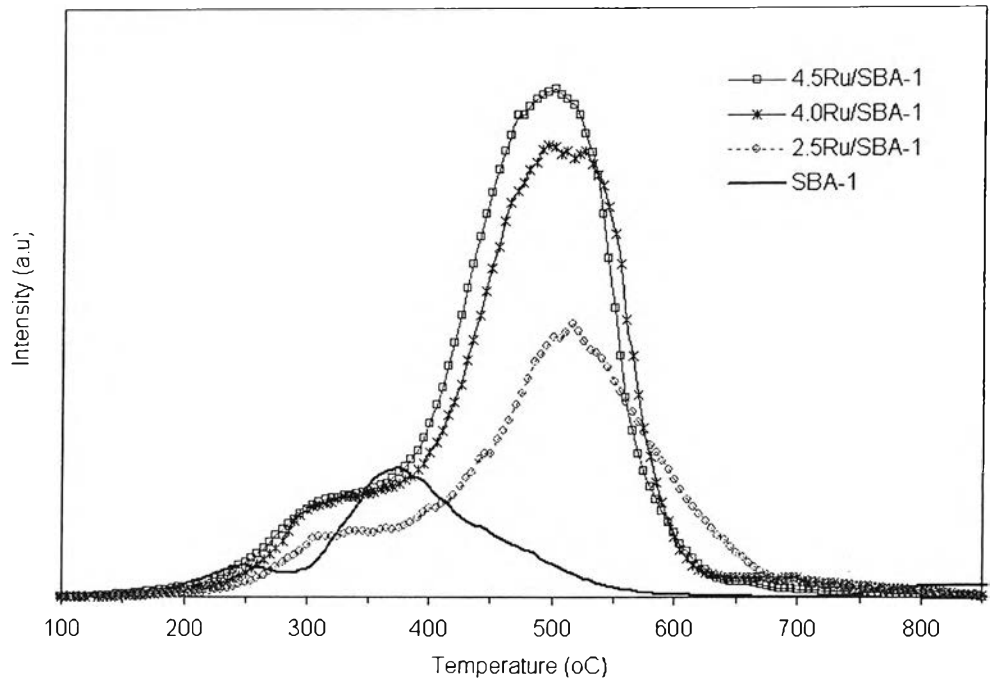

Figure 6.8 TPO of the spent Ru/SBA-1 catalysts.